

# The re-distribution of matter in the cores of galaxy clusters

Chervin F. P. Laporte<sup>1,2</sup> & Simon D.M. White<sup>1</sup>

<sup>1</sup> Max Planck Institute for Astrophysics, Karl-Schwarzschild-Strasse 1, 85740 Garching, Germany

<sup>2</sup> Department of Astronomy, Columbia University, 550 West 120th Street, New York, NY, 10027, U.S.A

## ABSTRACT

We present cosmological N-body resimulations of the assembly of the Brightest Cluster Galaxies (BCGs) in rich clusters. At  $z = 2$  we populate dark matter subhalos with self-gravitating stellar systems whose abundance and structure match observed high-redshift galaxies. By  $z = 0$ , mergers have built much larger galaxies at cluster centre. Their dark matter density profiles are shallower than in corresponding dark-matter-only simulations, but their total mass density profiles (stars + dark matter) are quite similar. Differences are found only at radii where the effects of central black holes may be significant. Dark matter density slopes shallower than  $\gamma = 1.0$  occur for  $r/r_{200} < 0.015$ , close to the half-light radii of the BCGs. Our experiments support earlier suggestions that NFW-like profiles are an attractor for the hierarchical growth of structure in collisionless systems – total mass density profiles asymptote to the solution found in dark-matter-only simulations over the radial range where mergers produce significant mixing between stars and dark matter. Simulated dark matter fractions are substantially higher in BCGs than in field ellipticals, reaching 80% within the half-light radius. We also estimate that supermassive black hole mergers should create BCG cores as large as  $r_c \sim 3$  kpc. The good agreement of all these properties with recent observational studies of BCG structure suggests that dissipational processes have not played a dominant role in the assembly of the observed systems.

**Key words:** galaxies: formation - galaxies: evolution - galaxies: clusters: general - galaxies: elliptical and lenticular, cD - cosmology: dark matter

## 1 INTRODUCTION

In the standard  $\Lambda$ CDM cosmological paradigm, dark matter is a collisionless particle and its clustering can be followed by solving the collisionless Boltzmann equation (CBE). This can be done using Monte-Carlo techniques such as the N-body method. In the last decade, cosmological dark-matter-only simulations have shown that the spherically averaged density profiles of dark matter haloes follow a universal form from clusters to dwarf galaxy scales which may be parametrised by the Navarro, Eke & Frenk (1996); Navarro, Frenk & White (1997, ‘NFW’ hereafter) profile<sup>1</sup>. This density profile falls off as  $\rho \propto r^{-3}$  at large radii and asymptotes to  $\rho \propto r^{-1}$  as  $r \rightarrow 0$ . The origin of this regularity is still unclear. Many arguments have been put forward, ranging from the effects of multiple mergers (Syer & White 1998) to the maximisation of en-

tropy subject to constraints like constancy of the actions (Pontzen & Governato 2013) but a convincing demonstration of the emergence of a universal profile is still lacking.

Observations of relaxed galaxy clusters, on the other hand, suggest that the dark matter density profiles in the innermost regions are shallower than those found in simulations (Sand et al. 2002, 2004, 2008; Newman et al. 2009, 2011, 2013b). Intriguingly, recent results from Newman et al. (2013a) combine a variety of mass measurement techniques (stellar kinematics, strong lensing, weak lensing and X-ray observations of the hot intracluster gas) to show that the *total* mass density profile in these regions (dark matter + stars + gas) does appear to be consistent with that found in dark-matter-only simulations. This has been interpreted as showing that although dissipational galaxy formation physics may compress or expand dark matter haloes during the early condensation and star formation phases, later collisionless merging re-establishes the NFW profile, which can thus be thought of as an attractor for the violent relaxation of collisionless systems. This hypothesis for the assembly of Brightest Cluster Galaxies (BCGs) was originally suggested by Loeb & Peebles (2003). Although

<sup>1</sup> It should be noted however that some scatter exists from halo to halo (Navarro et al. 2010) and the asymptotic slope may be go to lower values but at radii much smaller than the typical half-light radius of galaxies, by an order of 100.

baryon condensation into stars steepens the inner regions of the total density profiles of the progenitors, the many dissipationless mergers required to form the BCG take the combined collisionless fluid back to the universal profile found in dark-matter only simulations. Gao et al. (2004) explored this process qualitatively by tracking the central dark matter particles in dark matter-only simulations of galaxy clusters back to higher redshifts, demonstrating that the even the innermost dark matter distribution is indeed built up by the merging of a large number of separate entities present at higher redshift. They suggested that, in the presence of stars, efficient mixing would reestablish an NFW-like profile. However, an experiment containing two self-gravitating collisionless fluids (dark matter and stars) with initial conditions constrained by observations of real high-redshift galaxies needs to be carried out to test whether the attractor hypothesis is effective in a realistic situation.

It is generally thought that as dynamical friction brings the visible components of galaxies to cluster centre, it will evacuate dark matter from this region, pushing it to larger radii El-Zant et al. (e.g. 2004). However, dynamical friction and tidal stripping affect both the stars and the dark matter, both in the central object and in the galaxy which is merging with it. Laporte et al. (2012) showed that the competition between these processes can lead to different outcomes depending on the initial structure of high-redshift galaxies. In the simulations they analysed, these authors found that the mixing of stars and dark matter through dissipationless mergers did indeed reduce the slope of the dark matter cusp by up to  $\Delta\gamma = 0.5$  at the innermost resolvable radius, but their initial conditions were inconsistent with modern observations of high-redshift galaxies, so their results could only be interpreted qualitatively.

In this paper, we test whether the growth of galaxy clusters in a  $\Lambda$ CDM universe, starting from a  $z = 2$  galaxy population consistent with that observed, can produce realistic low-redshift BCGs, in particular, with dark matter cusps as shallow as those of Newman et al. (2013b) and total mass density and luminosity profiles consistent with (Newman et al. 2013a). We run simulations which explicitly emulate the compression of halo structure at  $z = 2$  caused by galaxy condensation, and we follow the subsequent evolution of the star and dark matter distributions fully self-consistently (under the hypothesis of no further star formation) to the present-day. To this end, we have developed a method for inserting self-consistent stellar components into dark matter haloes formed in a cosmological simulation. Past simulations of this sort have replaced dark matter haloes (and all their substructure) with spherical compound galaxy models made up of stars and dark matter (Dubinski 1998; Rudick et al. 2006; Ruszkowski & Springel 2009). We start with the  $z = 2$  output of a dark-matter only zoom-in simulation and insert equilibrium stellar spheroids directly into the centres of the dark matter subhaloes. Galaxy properties are as inferred from abundance matching results Moster et al. (2013) and from observed mass-size relations at  $z = 2$ . The systems re-equilibrate on a short timescale as the dark matter adjusts to the potential of the newly inserted stars, and thereafter the full system can be followed self-consistently to  $z = 0$  and the results compared to those of the original dark-matter-only simulation.

Section 2 introduces the original cluster simulations,

discusses our method for inserting equilibrium stellar components into their  $z = 2$  subhaloes, and tests that the results of this procedure are indeed stable, in the absence of merging, over cosmological timescales. We study the structural properties of our BCGs/clusters at  $z = 0$  in section 3. In section 4 we look more closely at the mergers and mixing processes that occur during the assembly of the central regions of the clusters, and we discuss the important role of black holes in section 5. Sections 6 and 7 provide further discussion and set out our conclusions, respectively.

## 2 NUMERICAL METHODS

### 2.1 Simulations

We use a suite of zoom-in dark-matter-only simulations of galaxy clusters, the PHOENIX project Gao et al. (2012) as our starting point for re-simulating the passive evolution of galaxies from  $z = 2$  to  $z = 0$ . The haloes in the PHOENIX suite were initially selected from the *Millennium Simulation* (Springel et al. 2005) and were re-simulated at a variety of resolutions. In this paper we use resolution level 2 simulations of two of the nine Phoenix clusters (simulations Ph-C-2 and Ph-E-2 in the original notation). These have co-moving softening length  $\epsilon = 0.3 h^{-1}$  kpc and mass resolution  $m_p \sim 4 - 10 \times 10^6 h^{-1} M_\odot$ . Further details of the simulations are given in Gao et al. (2012). They adopt the cosmology of the original Millennium Simulation:  $\Omega_m = 0.25$ ,  $\Omega_\Lambda = 0.75$ ,  $\sigma_8 = 0.9$  and  $n = 1$ . These parameters are outside the range currently considered plausible, but this is of no consequence for the current paper. For the rest of the discussion, our spatial and mass units are in kpc and in  $M_\odot$  respectively (i.e. no  $h$ ). Subhaloes were identified using the SUBFIND algorithm (Springel et al. 2001). We insert equilibrium models of the stellar components of galaxies into the dark matter subhaloes of the original simulations at  $z = 2$ , and follow the later evolution of the stellar and dark matter distributions down to the present-day. For these resimulations we keep the softening lengths for star and dark matter particles fixed in physical units at  $\epsilon = 0.1$  kpc, corresponding to the softening of the original dark matter simulation at  $z = 2$ .

### 2.2 Generating the stellar components of pre-existing halos

The galaxies are represented by Hernquist (1990) spheres:

$$\rho_* = \frac{a M_*}{r(r+a)^3}, \quad (1)$$

where  $a$  is the scale radius which is related to the 3D half-mass radius through  $a = r_e/(\sqrt{2} + 1)$ . The half-mass radius in projection is related to  $r_e$  through  $R_e = r_e/1.33$ .

Initially spherical N-body models for the stellar distributions are generated through Monte Carlo sampling of an isotropic distribution function (DF) of the form  $f \equiv f(E)$  using a von Neumann rejection technique (Kuijken & Dubinski 1994; Kazantzidis et al. 2004). The DF takes the form:

$$f_*(\mathcal{E}) = \frac{1}{\sqrt{8\pi^2}} \int_0^\mathcal{E} \frac{d\Psi}{\sqrt{\mathcal{E} - \Psi}} \frac{d^2\rho_*(\Psi)}{d\Psi^2} + \frac{1}{\sqrt{\mathcal{E}}} \frac{d\rho_*}{d\Psi} \Big|_{\Psi=0}, \quad (2)$$

where  $\Psi = -\Phi + \Phi_0$  and  $\mathcal{E} = -E + \Phi_0 = \Psi - v^2/2$  are the potential relative to halo centre (containing the contributions of both dark matter and stars) and the specific orbital energy, respectively. The potential of the dark matter halo is modelled as that of the Hernquist sphere which best fits (in a  $\chi^2$  sense) the spherically averaged density profile of the halo. Because the total potential is modelled as the superposition of two Hernquist spheres, the second term in equation 2 drops out. While there are better ways to represent the potential of the dark matter haloes, we have found this approximation to be robust enough to produce stable galaxies (as will be shown later). Moreover, we note that although it is often recommended to take account of the Plummer softening when generating N-body models from distribution function based methods, in the case of a Hernquist potential, Barnes (2012) demonstrates that this is not necessary provided the softening length is smaller than the scale radius of the galaxy and that the stellar profile is not strongly centrally cusped (e.g.  $\rho_* \propto r^{-2}$ ). The spherical equilibrium stellar distribution produced by this procedure is centred on the potential minimum of simulated halo and given a mean velocity equal to that of the halo's inner regions.

### 2.3 Stability tests

We perform some stability tests to check whether our method works properly. We extract a subhalo identified by SUBFIND at  $z = 2$  in the cosmological dark-matter-only run of Ph-E-2, and we insert a spheroid with stellar mass and size determined as described in the next subsection. We then evolve this system in isolation with a fixed physical softening length of  $\epsilon = 0.1$  kpc for a period of 10 Gyr. The dark matter contracts on a timescale of 200 Myr due to the gravitational effects of the impulsively imposed stellar component, but the stellar component itself varies much less because its own potential was included when initialising particle velocities. This is shown in Figure 1 which shows that even after 10 Gyr the half-light radius of the galaxy has only changed by  $\sim 10\%$  and its luminosity profile is still quite similar to that set up initially. The initial change of the dark profile can be seen in Figure 2. There is a substantial steepening throughout the region occupied by stars, but this compressed profile is then stable over Gyr periods. The nonspherical shape of the dark matter halo also induces a flattening of the stellar component after re-virialisation, as shown in Figure 3. We have not attempted to prevent the rapid contraction of the dark matter component, considering that the ‘adiabatically compressed’ dark matter profile of the later panels of Figure 2 is as likely to be realistic as any alternative which we could set up. Note that this initial contraction implies that the dark matter distributions of our galaxies have significantly *steeper* inner profiles (and the total mass distributions substantially steeper inner profiles) than the corresponding objects in the dark-matter-only simulation. This makes all the more remarkable the relaxation towards NFW total mass profiles which we demonstrate below.

This method improves significantly on past attempts to embed galaxies in dark-matter-only cosmological simulations. These typically replaced entire simulated dark matter haloes by idealised equilibrium models of a galaxy embedded in a smooth and spherical dark matter halo Dubinski (1998); Rudick et al. (2006); Ruszkowski & Springel (2009),

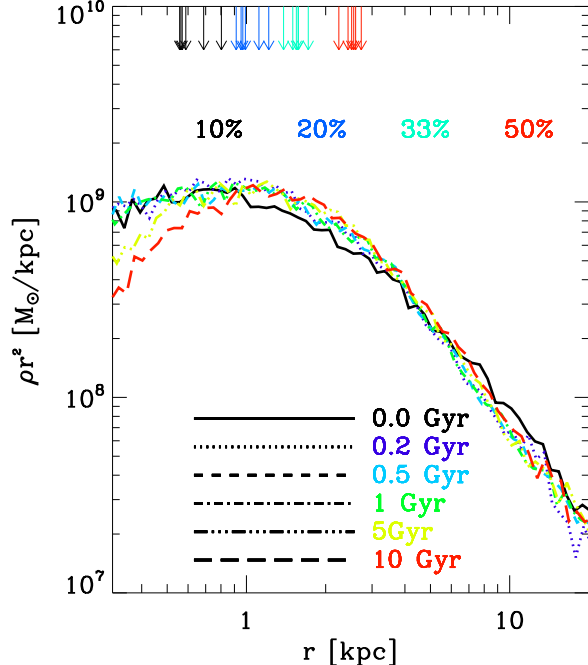


**Figure 1.** Evolution of the stellar density profile in our stability test. Using the machinery described in the text, we introduce a stellar component in a live dark matter halo which we evolve in isolation. The system undergoes a rapid phase of re-virialisation which only slightly changes the stellar density profile. Thereafter it changes very little over 10 Gyr of evolution. Arrows mark the radii enclosing 10, 20, 33 and 50 percent of the light, these increase with time, but the overall increase in half-light radius is of order 10 percent. This galaxy has a dark halo mass of  $M_h = 7 \times 10^{12} M_\odot$ , a stellar mass of  $M_* = 9 \times 10^{10} M_\odot$  and a half-light radius of  $r_e \sim 2.5$  kpc

thus losing the true shape and the substructure of the original halo and causing artifacts at the boundaries between embedded haloes and their surroundings. In our experiment, the original halos are retained and settle into new quasi-equilibrium configurations after a few central dynamical times. In addition, recent improvements in computer capabilities mean that we are able to carry out experiments of significantly higher resolution than was previously possible, allowing us to follow the structure of galaxy/halo systems realistically down to subkiloparsec scales. Based on a series of tests similar to that illustrated here but for galaxies of different stellar mass, we conclude that we can reliably follow the structural evolution of galaxies with  $M_* \geq 2 \times 10^{10} M_\odot$  without the effects of softening or two-body relaxation compromising our results.

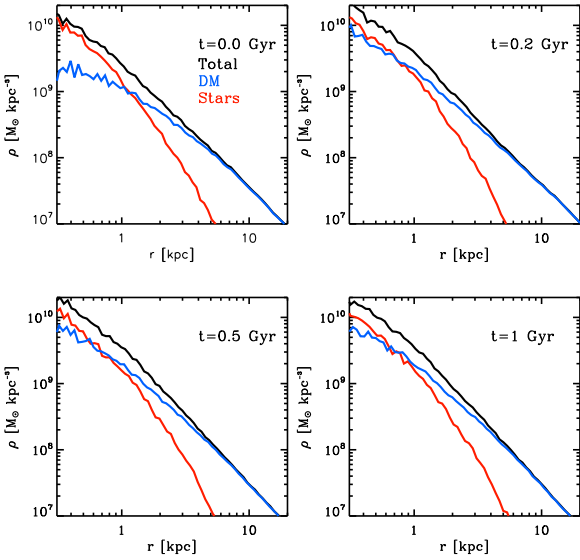


**Figure 2.** Evolution of the density profiles of the stars (red), the dark matter (blue) and the total mass (black) in our stability test. The system stabilises quickly after an initial contraction of the dark matter on a timescale of  $t \sim 200$  Myr.

#### 2.4 Initial conditions

Using the method described above, we put galaxies at the centres of all  $z = 2$  subhaloes in the original dark-matter-only simulations which are expected to host galaxies with  $M_* > 2 \times 10^9 M_\odot$ . We wish to insert a galaxy population that agrees closely with that observed at  $z = 2$ . The stellar mass of each galaxy is therefore chosen so that it lies on the  $M_{200} - M_*$  relation inferred from the abundance-matching analysis of Moster et al. (2013). Its size is then set according either to the mass-size relation for red, compact, massive and quiescent galaxies or to that of extended, blue, star-forming galaxies as given by van der Wel et al. (2014). The choice between the red and blue relations is made in a probabilistic way using the observed fraction of quiescent  $z = 2$  galaxies as a function of stellar mass from Muzzin et al. (2013) which is determined down to  $10^{10} M_\odot$ . Below this stellar mass, sizes are selected according to the overall scatter in the mass-size diagram of galaxies (which is substantial). The result is illustrated in Figure 4. Although it is clearly still an approximation to represent all galaxies as Hernquist spheres, our experiment is still realistic in that it assigns every dark matter subhalo a galaxy with a stellar mass and size which are consistent with observations of  $z = 2$  galaxies.

#### 2.5 Cluster simulations

We have resimulated two cluster mass haloes from the Phoenix suite. These are the Ph-E-2 and Ph-C-2: their properties are summarized in Table 1. Before starting a detailed presentation of our results, it is useful to understand where the material which makes up the central  $r < 10\text{kpc}$  of the

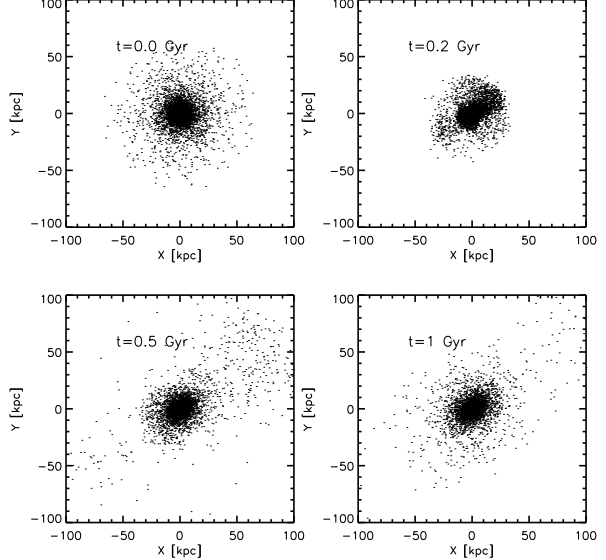


**Figure 3.** Projected images of the stellar component of the same galaxy as in Figure 1 and 2, showing the flattening induced by the re-virialisation process. The stellar distribution is centred on the potential minimum of the dark matter halo, and the mean velocity of the 100 most bound dark matter particles is added to that of each of the stars to ensure that galaxy and halo are initially moving together. The image illustrates that the time-dependent inner structure of real dark matter haloes can drive some initial transients in the stellar distribution, but these lead to relatively minor long-term effects.

Run	$M_{200}$ $h^{-1} M_\odot$	c	$R_{200}$ $h^{-1} \text{Mpc}$
Ph-C-2	$5.495 \times 10^{14}$	5.11	1.386
Ph-E-2	$5.969 \times 10^{14}$	5.19	1.369

**Table 1.** Basic structural properties (virial mass  $M_{200}$ , concentration  $c$  and virial radius  $R_{200}$ ) of the Phoenix clusters at  $z = 0$  from the original dark-matter-only simulations.

final system actually comes from. This is shown in Figure 5, which illustrates graphically that the inner regions of BCGs are expected to be built up from a significant number of disjoint objects, as already pointed out using similar plots by Gao et al. (2004). In Figure 11 below we will show that this is true for the stars as well as for the dark matter.

### 3 STRUCTURE OF GALAXY CLUSTERS

#### 3.1 Density profiles

In this section we present  $z = 0$  inner density profiles for the stellar and dark matter components of our two simulations and for their sum. We compare these to the profiles found in the corresponding dark-matter-only simulations. These are plotted in Figure 6 in the form of normalised  $\rho r^2 / (\rho_{200} r_{200}^2)$  profiles as a function of normalised radius  $r/r_{200}$ . Overplot-

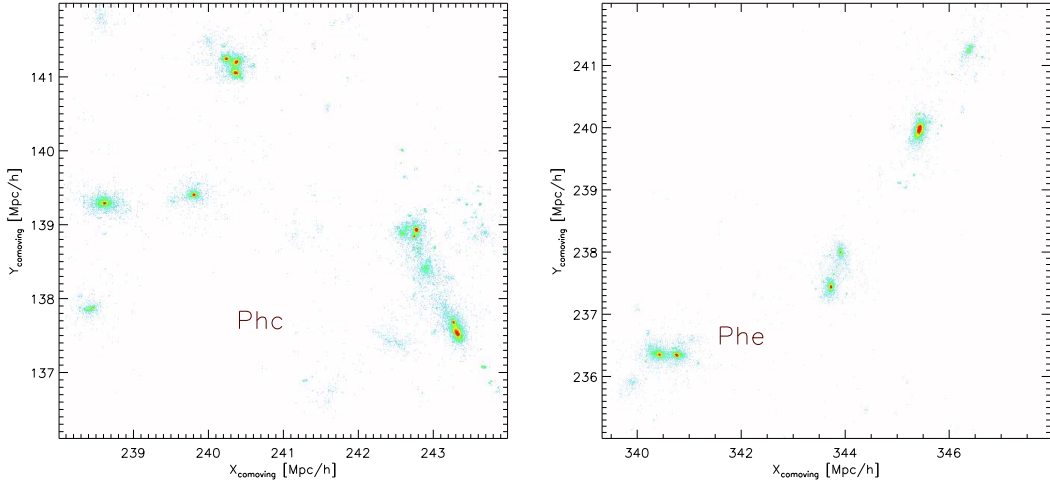


**Figure 5.** Distribution at  $z = 2$  of the dark matter particles which at  $z = 0$  lie within 10kpc of cluster centre in the original *Phoenix* simulations Ph-C-2 (left) and Ph-E-2 (right). This illustrates that even the very central regions of galaxy clusters are typically in many disjoint pieces at  $z = 2$ .

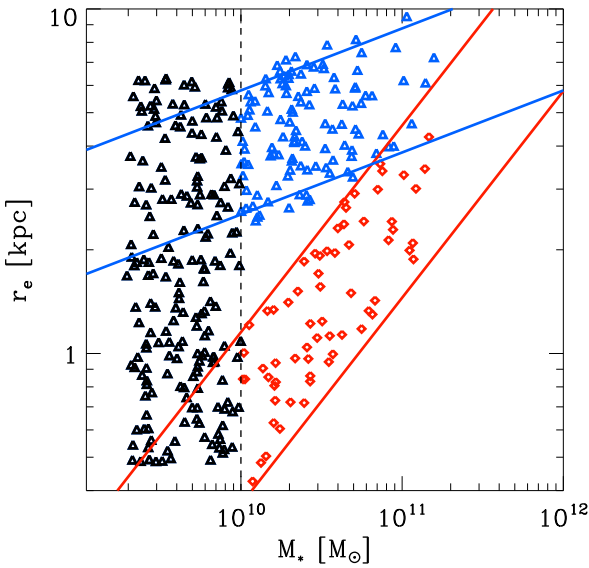


**Figure 4.** Mass-size relation of the galaxies we insert into the Ph-E-2 simulation. Red symbols have properties set according to the observed relation for compact, massive, quiescent galaxies, while blue ones follow the observed relation for the massive, star-forming galaxies. Below  $10^{10} M_\odot$ , observational classifications are uncertain so we mimic the overall observed scatter in size (black triangles).

ted on the simulations in this figure are the profiles derived by Newman et al. (2013a,b) for their sample of real clusters. The first interesting result to note is that the total density profiles in the dark-matter-only and star+dark matter runs look very similar despite the fact that they started out very different (compare the blue and black profiles in the top

left panel of Figure 2). The only clear difference at  $z = 0$  is in the innermost regions of the BCG. Furthermore, although the dark matter distributions after revirialisation are clearly more centrally concentrated at high redshift in the star+galaxy run than in its dark-matter-only counterpart (compare the blue curve in the top left panel of Figure 2 with those in the other three panels) the opposite is true in the final object, where the dark matter profile in the simulation with stars dips below that in the simulation without stars for radii  $r < r_{200} \sim 0.01 - 0.02$ , approximately the 3D half-light radius of the final BCG ( $r_e \sim 30$  kpc for Ph-C-2 and  $r_e \sim 18$  kpc for Ph-E-2, as shown by the red arrows). The stellar density profile is also in reasonable agreement with the observed stellar profiles of Newman et al. (2013a). Since our simulations assume purely dissipationless evolution since  $z = 2$ , this suggests that star formation at lower redshifts may not play an important role in the structuring of BCGs.

In Figure 7, we present density profile slopes, defined as  $\gamma = -\frac{d \ln(\rho)}{d \ln(r)}$  as a function of normalised radius  $r/r_{200}$ . In computing the slopes we have binned our data between  $r = 0.1$  kpc and  $r = 1000$  kpc into logarithmic bins of width  $\Delta \log(r) = 0.1$ . We have tried other binning schemes, finding they all lead to consistent results. The slopes of our BCG stellar profiles are roughly consistent with those measured, although they may be systematically steeper at small radii  $r/r_{200} < 0.002$ . The slopes of the dark matter density profiles in our resimulations are systematically shallower than those of the original dark-matter-only runs. The radius where these become shallower than the asymptotic NFW value (represented by the horizontal dash-dotted line) is  $r \sim 0.01 r_{200}$  which agrees with that found observationally ( $0.01 < r/r_{200} < 0.03$  according to Newman et al. (2013b)). This scale also corresponds closely to the BCG half-light radius. Turning to the total density profiles, these also match those observed by Newman et al. (2013a) except in the innermost regions ( $r < 0.002 r_{200}$ ) where they clearly become steeper. It seems that mixing is efficient enough to cause ap-

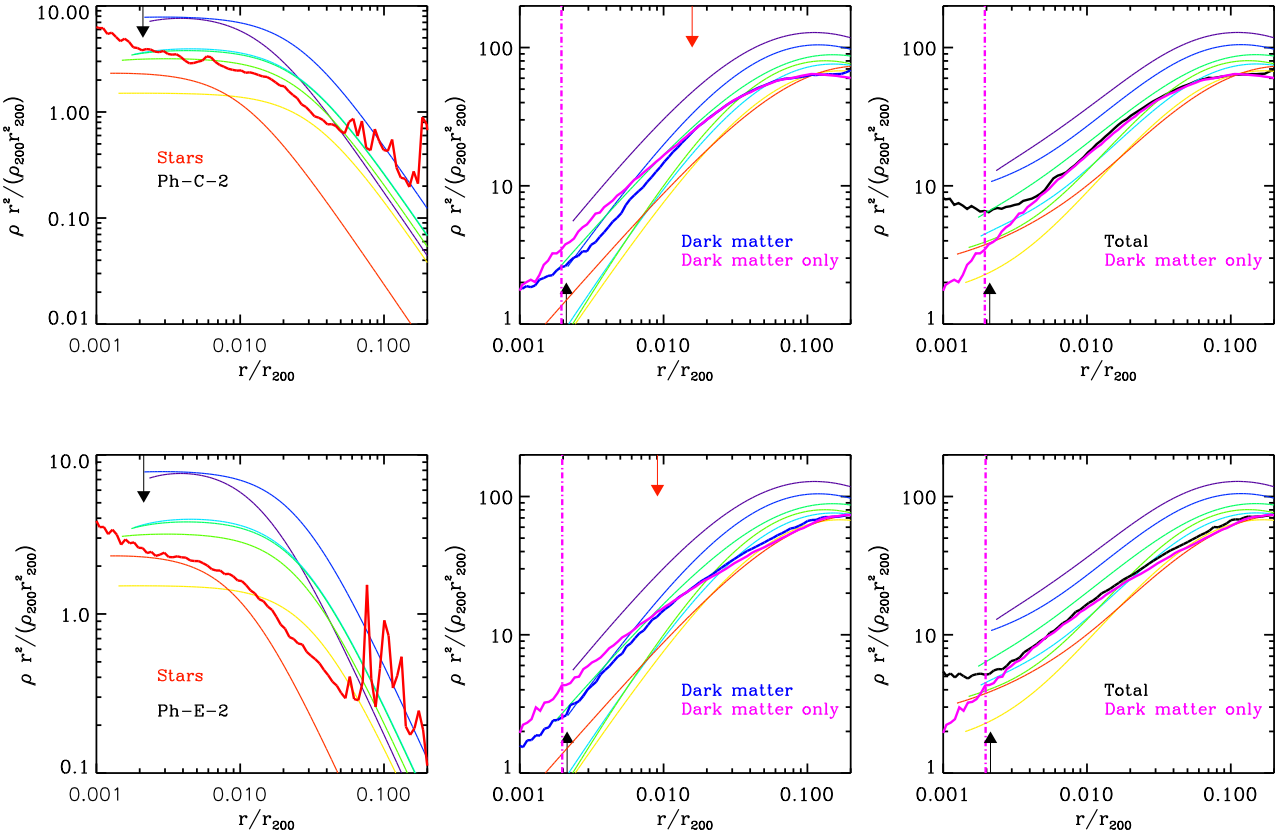


**Figure 6.** Heavy lines in each panel show  $\rho r^2$  profiles for the clusters normalised by  $\rho_{200} r_{200}^2$  as a function of normalised radius  $r/r_{200}$  for the stars (left panel in red), for the dark matter (middle panel in blue) and for their sum (right panel in black). Thinner coloured lines show profiles for observed clusters from Newman et al. (2013a,b). The magenta lines in the middle and right panels show the profiles found in the original dark-matter-only simulations. The inclusion of stars has clearly caused a drop in the dark matter density at radii within  $r \sim 10$  kpc. In contrast, the total mass profiles are very similar in the two cases, even well inside the half-light radii of the galaxies. Differences are only substantial in the innermost regions where the stellar density exceeds that of the dark matter. Black arrows mark the radii where a mass deficit (in the form of a core) would be expected due to black hole mergers (see section 6.4). Red arrows mark the half-light radii of the BCGs, which turn out to be close to the radii where the slope of the dark matter profile becomes shallower than  $\gamma = 1$ .

proach to an attractor solution down to radii well within the half-light radii of the BCGs.

### 3.2 Velocity Dispersion Profiles

In Figure 8, we compare projected stellar line-of-sight velocity dispersion (LOSVD) profiles for our BCGs (based on 100 random projections) to observations from Newman et al. (2013b). We observe a very similar rise in LOSVD with radius as reported by Newman et al. (2013a) for their observed clusters, with central velocity dispersion  $\sigma \sim 300$  km/s and outer velocity dispersion  $\sigma \sim 400.0$  km/s. We note that the scatter in velocity dispersion profile due simply to projection is quite substantial, with *rms* variations of 10 to 15%. Given that both the structure and the kinematics of the simulated BCGs seem to agree well with observation, it is interesting to investigate in greater detail how multiple mergers shape the distributions of dark and stellar matter in the inner regions of galaxy clusters.

### 4 MERGERS, MIXING & DARK MATTER HEATING

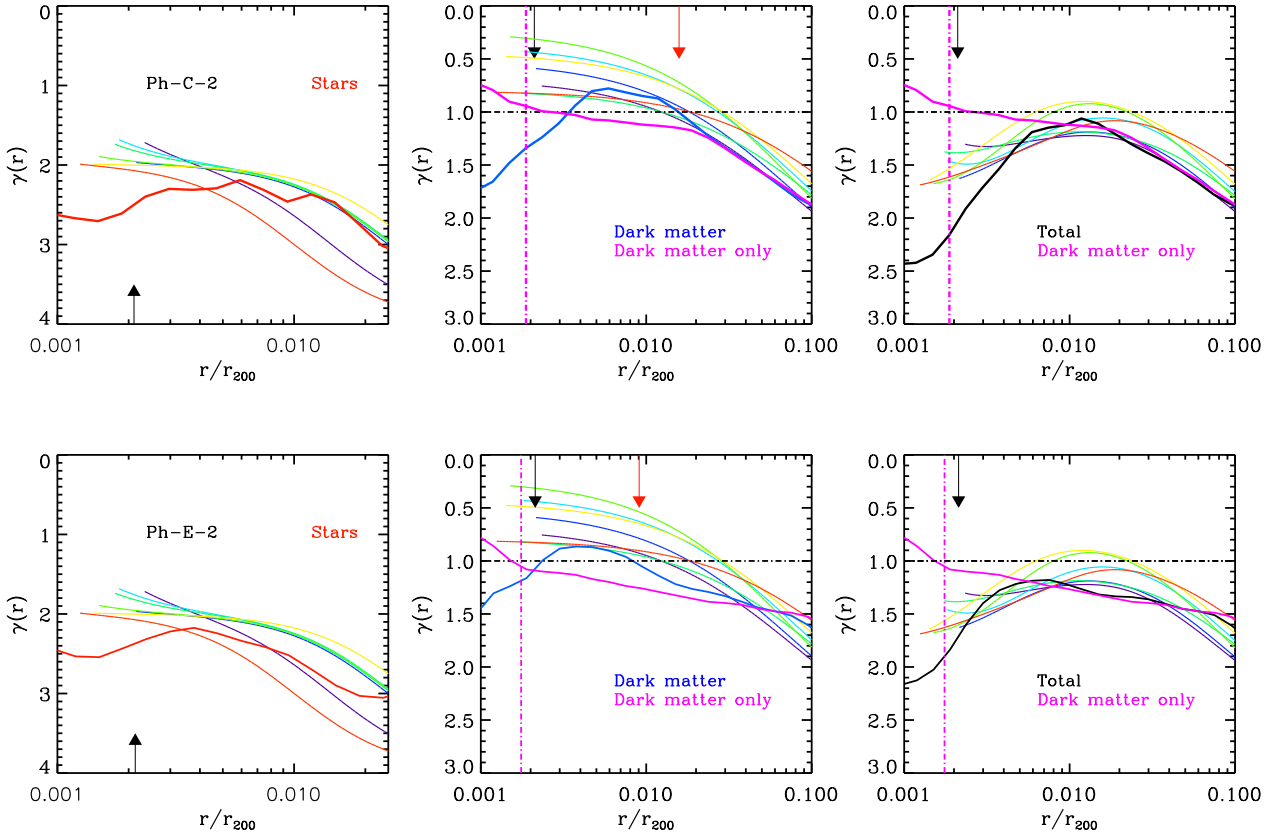


**Figure 7.** Density profile slopes as a function of normalised radius  $r/r_{200}$  in the same format as Figure 6. Coloured lines are the slopes obtained for real clusters by Newman et al. (2013a,b). For the total mass, the agreement between observation and our resimulations is reasonably good (right panel). The dark matter slopes in our resimulations are clearly shallower than in the dark-matter-only runs (blue and magenta lines in the middle panel) and the scale at which they become less than  $\gamma = 1$  is similar to that found by Newman et al. (2013b) for real clusters, corresponding to physical radii of  $r = 18 - 30$  kpc. Slopes for the stars are steeper and are also similar to those measured by Newman et al. (2013b). Black arrows mark the radii where we estimate that a mass deficit (in the form of a core) due to black hole mergers should become appreciable (see section 6.4). Red arrows mark the half-light radii of the BCGs, which are similar to the radii within which  $\gamma < 1$  for the dark matter.

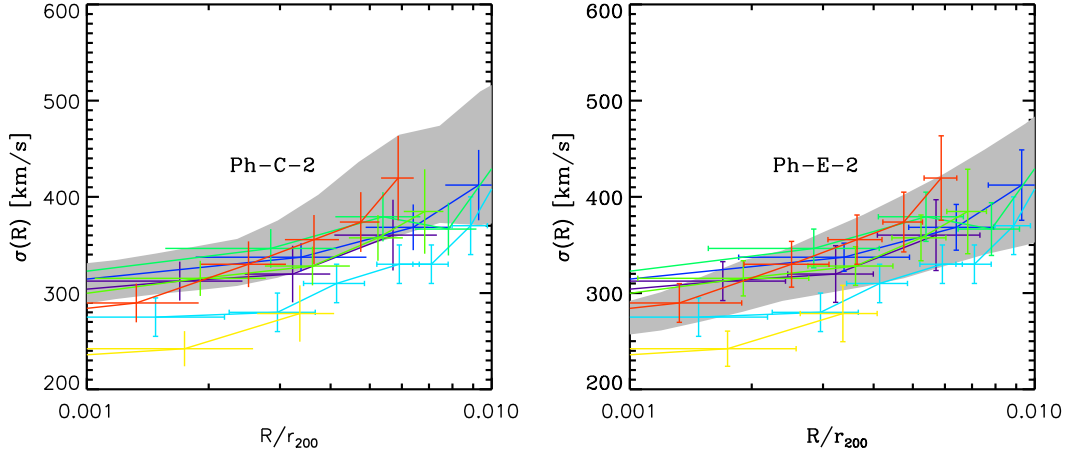
In this section, we investigate in more detail how repeated mergers cause dark matter profiles to get shallower at small radius and total mass profiles to converge to NFW-like form. We proceed by selecting particles which at  $z = 0$  have binding energy  $E < E_0$ , placing them at the centre of the final galaxy cluster.  $E_0$  is chosen so that most of the particles with  $r < 100$  kpc are included. We then track these particles back to  $z = 2$  and separate them according to the progenitor objects to which they belong. We consider the most massive of these to be the “main” progenitor of the final BCG. We then follow these sets of particles forwards in time studying how they contribute to the build up of the stellar and dark matter distributions of the final BCG. In Figure 11 we show images of the distribution of the stellar particles selected in this way at a series of redshifts which we analyse in more detail below. Colored stars in this plot indicate individual progenitors using the same colour scheme as in the profiles of Figure 9, which we discuss next. Clearly, BCG progenitors can be widely separated at  $z = 2$ .

Figure 9 itself takes the form of a time series of  $\rho r^2$  density profiles, picking times which are particularly illustrative

of the way in which mergers induce changes in structure. In these plots, thick black lines indicate profiles from material which was part of the main ‘ $z = 2$ ’ progenitor while colored lines are for material from other progenitors. The colours correspond between times and solid and dashed lines indicate objects which at  $z = 2$  were central and satellite galaxies, respectively. The black dash-dotted lines show profiles for all the stellar/dark matter particles without separation by binding energy or origin. Dotted lines show profiles for material from objects which contribute fewer than 100 particles at  $r < 5$  kpc (individual profiles are only shown for objects where this is not the case). Because of the complexity in merging history and progenitor properties (stellar mass and size) we will discuss the plots for each resimulation individually.

#### 4.1 Ph-C-2: dark matter heating with no re-shuffling

Between  $z = 2$  and  $z = 1$  the main progenitor of this cluster interacts with a number of galaxies which substantially



**Figure 8.** Projected stellar velocity dispersion as a function of projected radius (normalised by  $r_{200}$ ) computed for 100 random orientations of our two  $z = 0$  BCGs. The grey area shows the  $1\sigma$  scatter in velocity dispersion due to projection effects. Overplotted are the velocity dispersions measured by Newman et al. (2013a) for seven of their clusters.

modify the shape of its dark matter profile, mixing it with material from larger radii and from other objects. By  $z = 1$ , one large galaxy has merged to the centre and the system has relaxed to produce a dark matter density profile which is already substantially shallower than initially (compare the dash-dotted curves in the top left two panels of Figure 9 and see also Figure 10). The merging galaxy has brought in a significant amount of dark matter which contributes at least as much to the profile as the main progenitor at all radii (compare grey and black curves in the second and third panels of the top row of Figure 9). The stars from the merging galaxy only dominate the merger product beyond about 5 kpc, however. A number of other significant mergers occur after  $z = 0.4$ , note it is only after  $z = 0.1$  that another merger occurs that effects the innermost regions of the final BCG. Dark matter from this last merging galaxy dominates the final profile within a few kpc, and its stars contribute equally to those of the main progenitor within about 10 kpc (compare the red and black curves in the  $z = 0$  panels). Stars contributed by other progenitors are only significant at larger radii. The shallow dark matter profile established by  $z = 0.4$  is counteracted slightly at the very centre by this last merger but is maintained at all larger radii. In this cluster it is notable that stars from the main progenitor dominate the inner regions of the BCG at all times except the last one, and even then they contribute substantially down to the smallest radii.

#### 4.2 Ph-E-2: dark matter heating with re-shuffling

The inner regions of this cluster show a very different assembly history than Ph-C-2. Between  $z = 2$  and  $z = 1$ , there is very little merging activity. Essentially no stars are added to the central galaxy and the small amount of additional dark matter comes from mixing processes and from a few objects which were disrupted at relatively large radius. Nevertheless, many satellites are orbiting the central galaxy at somewhat larger radii, and this causes some mixing and

heating which causes both the stellar and dark matter profiles of the central galaxy to become somewhat shallower. Between  $z = 1$  and  $z = 0.9$  one of these satellites merges with the central galaxy (see the yellow curves in the  $z = 0.9$  panels – the satellite is visible as a spike at  $\sim 45$  kpc in the  $z = 1$  panels) inducing a further small decrease in the slopes of the stellar and dark matter profiles. Shortly thereafter, another galaxy (indicated by light blue curves) merges with the BCG and for a short period contributes the dominant stellar population near its centre. By  $z = 0.5$ , however, two additional galaxies (indicated by dark blue and red curves) have merged together, and have usurped the old BCG to become the bottom of the cluster potential well. The old BCG with its multiple components can be seen as a concentration at  $r \sim 10$  kpc from this new centre which is disrupted into the envelope of the system at later times (see the  $z = 0$  panel). The two progenitors which dominate the BCG at  $z = 0.5$  contribute almost equally to its dark matter content in the inner few kpc, but the stars in this region are contributed almost entirely by one of the two (indicated by red curves) which had the more compact initial galaxy. Finally, by  $z = 0$  yet another galaxy (indicated by green curves) has merged into the BCG and dominates its stellar and dark matter content in the central regions.

The underlying reason for this constant reshuffling is that mergers tend to reduce the mass density in the inner regions of the BCG, and as a result new inspiralling satellites can make it all the way into the central regions without being disrupted provided they are initially relatively compact. Thus the “older” BCG material is continually pushed outwards as it is heated by the incoming objects which are replacing it. This competition leads to the inner regions of the final object being preferentially composed of stars that came from compact progenitors which were added relatively late.

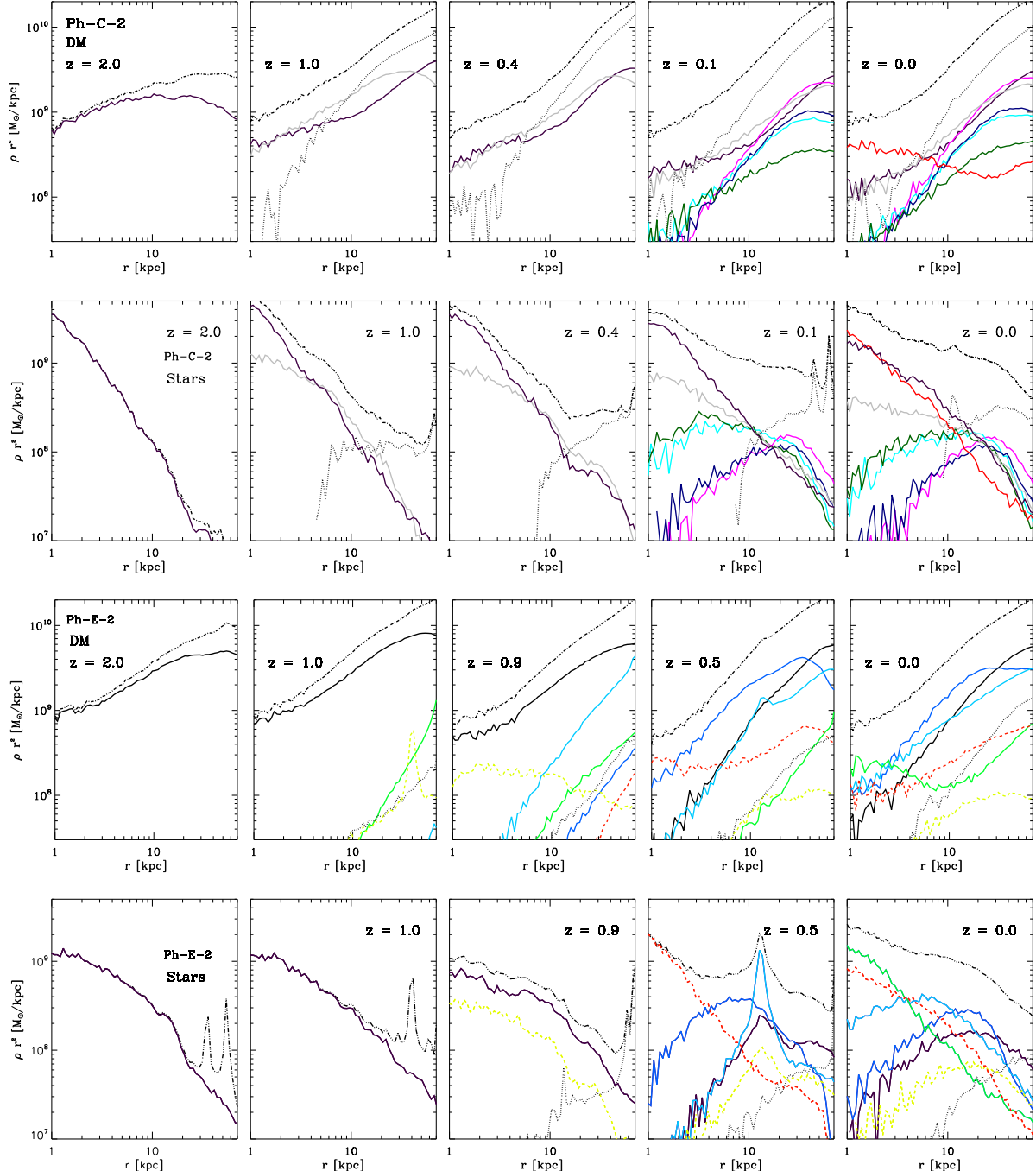


**Figure 9.**  $\rho r^2$  profiles as a function of radius for the dark matter and stellar components of our two clusters for particles with energy  $E < E_0$  at  $z = 0$ . The top two rows are for Ph-C-2, while the bottom two rows are for Ph-E-2. In each pair, the upper row gives dark matter profiles while the lower row gives stellar profiles. A thick black solid line in each panel designates the component associated with the most massive progenitor at  $z = 2$ . Colored lines are for particles belonging to other  $z = 2$  progenitors. Central and satellite objects at  $z = 2$  are distinguished by solid and dashed lines, respectively. Only profiles associated with  $z = 2$  progenitors which have brought more than a 100 particles within 5 kpc are plotted to avoid over-crowding. Black dotted lines are profiles for all the stars and for all the dark matter at each time are plotted as dashed-dotted lines.

#### 4.3 The evolution of density profile slopes

The effects of merging activity on the dark matter profile slope in the inner regions of our two clusters can be seen more easily in Figure 10, where this slope is plotted against radius for the specific redshifts shown in Figure 9. These

curves thus show the logarithmic derivative of the dash-dotted curves in the dark matter panels of Figure 9. A horizontal dotted line at  $\gamma = 1$  indicates the asymptotic inner slope of an NFW profile.

In our initial conditions  $\gamma$  is substantially larger than

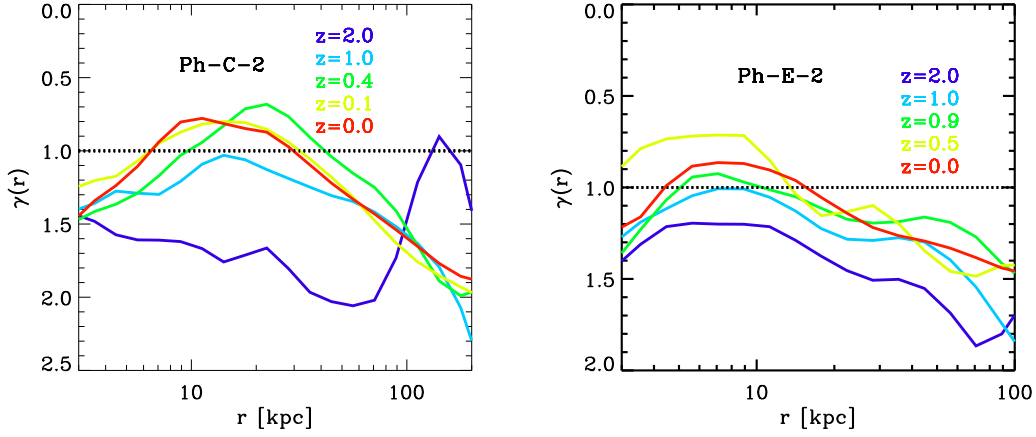


**Figure 10.** Evolution of the slope of the dark matter profile as a function of radius for our two clusters. The times correspond to those of Figure 9. *Left:* Ph-C-2: A first merger before  $z = 1$  has already brought the slope to quite shallow values and a later one below  $z = 0.4$  establishes a shallow dark matter cusp which is preserved though other mergers and extends with  $\gamma < 1$  from 6 to 30 kpc at  $z = 0$ . *Right:* Ph-E-2: A similar behaviour is seen where the slope of the dark matter gets shallower after each merger. Close to a merger this is more extreme (yellow line) but the system always relaxes to a shallower dark matter slope which by  $z = 0$  has  $\gamma < 1$  from 4 to 15 kpc.

one at all radii and in both simulations, reflecting the steepening of the dark matter profile caused by contraction in response to the gravitational effects of the added stars. By  $z = 1$  the inner dark matter profiles have become substantially shallower, however, reaching  $\gamma = 1$  in both cases, and this trend continues so that  $\gamma < 1$  over substantial regions by  $z = 0$ ,  $6 \text{ kpc} < r < 30 \text{ kpc}$  for Ph-C-2 and  $5 \text{ kpc} < r < 15 \text{ kpc}$  for Ph-E-2.

#### 4.4 Dark matter fractions

Although we have simulated only two clusters, it is clear that allowing initial galaxies to have a range of structural properties at given mass combines with the stochasticity of merging histories to produce very different amounts of mixing and hence a wide range of dark matter fractions in the final BCGs. We study this as function of radius and redshift in Figure 12. There are several ways of looking at the dark matter fractions. One may be interested in their variation over a given radial range of the galaxy, which is determined by how mergers affect the relative amounts of stars and dark matter within a fixed physical scale. Alternatively, it may be more helpful to consider the evolution of the dark matter fractions within a region which encloses a given fraction of the BCG's stars, for example, within its half-light radius. Such variations are directly related to mixing during the growth in size and mass of the galaxy. Both types of variation can be seen in Figure 12 for the BCG's in our two simulations.

For Ph-C-2 the dark matter fraction as a function of radius evolves relatively modestly, decreasing with time at all but the smallest radii. However, the dark matter fraction within the half-light radius increases substantially as the system evolves, from 0.1 at  $z = 2$  to 0.8 at  $z = 0$  (indicated by the values at which the black and red arrows intersect the mass fraction curves at  $z = 2$  and  $z = 0$  re-

spectively). In contrast, the evolution in Ph-E-2 is stronger at fixed radius, but much milder within the half-light radius, increasing from  $f_{DM} = 0.65$  to  $f_{DM} = 0.75$  over the same redshift range. This illustrates that dissipationless mergers can alter the dark matter fraction within BCGs, but the amount varies greatly from system to system because of the diversity of structural properties in the progenitor galaxies. Indeed, while the dark matter fraction in the innermost regions of Ph-C-2 increases with time, that in Ph-E-2 decreases substantially from  $z = 2$  to  $z = 2$  because at late times these regions are dominated by material from a small object that merged with the BCG at  $z \sim 0.8$  and had much higher stellar density than the main BCG progenitor (compare with Figure 9). Interestingly, despite the very different merger histories of our two BCG's, the final dark matter fraction within the half-light radius agrees well for both with estimates from Newman et al. (2013b) who find  $f_{DM} \sim 0.8$  within the effective radii of their observed BCG sample.

## 5 THE EFFECTS OF SUPERMASSIVE BLACK HOLES

Given the substantial number of mergers occurring during the formation of BCGs in  $\Lambda$ CDM, it is worthwhile to consider how the presence of supermassive black holes may affect the central distribution of dark and stellar matter. While the experiments of this paper do not specifically include supermassive black holes, we can still use observed relations between the mass of central black holes and that of their host galaxy to estimate the potential importance of black hole mergers in re-distributing matter in the inner regions of BCGs. Although quite rough, such estimates are useful to give an idea of the size of the regions which may be affected.

The BCG in Ph-E has experienced five mergers which have brought significant stellar material to the centre of

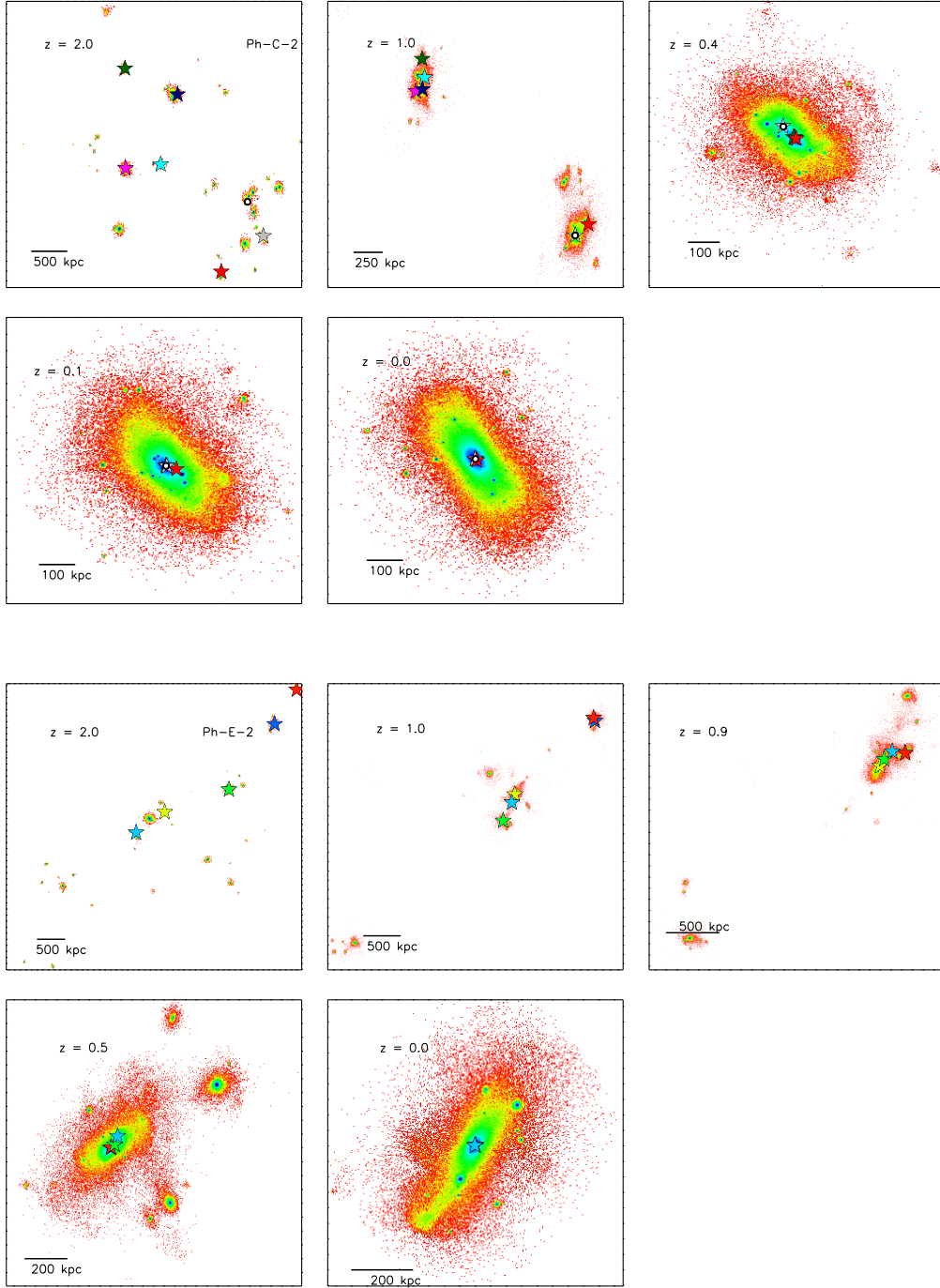


**Figure 11.** Distribution at a series of redshifts of stellar particles selected to have  $E < E_0$  at  $z = 0$ . Only galaxies contributing more than 100 particles to the central 5 kpc of the final BCG are shown. The top panels are for Ph-C-2 and the lower ones for Ph-E-2. Stars identify individual progenitors and are colour-coded to correspond to the curves in Figure 9.

the galaxy. From the initial stellar masses of the progenitor galaxies, we can estimate the masses of the black holes they host. We do this using the relation published by Bennert et al. (2011):  $\log(M_\bullet) = \alpha(\log(M_*) - 10) + \beta \log(1+z) + \gamma + \sigma + 8$ , with  $\alpha = 1.09$ ,  $\beta = 1.96$ ,  $\gamma = -0.48$ ,  $\sigma = 0.36$ . When two galaxies merge, their central black holes are assumed to merge also, and in its later stages the in-spiral of

the binary black hole deposits energy in the inner regions of the stellar merger remnant, giving rise to an apparent ‘mass deficit’ relative to the structure expected in the absence of the black holes. Merritt (2006) used N-body simulations to study this process and to relate the size of this stellar mass deficit to the masses of the merging black holes. He found  $M_{\text{def}} \sim 0.5M_{12}$ , with  $M_{12} = M_1 + M_2$  the total mass of the

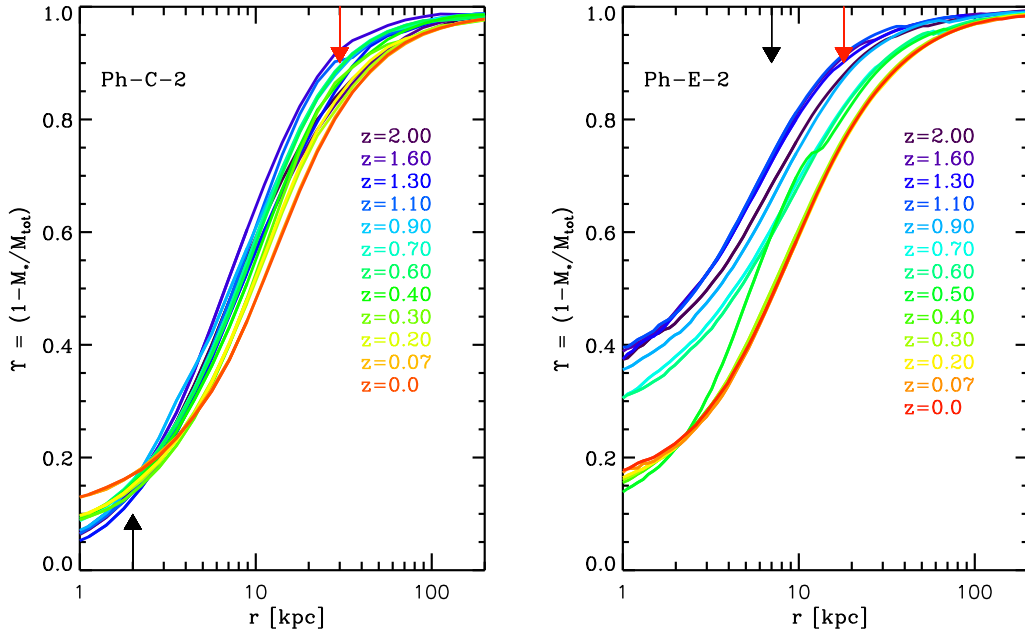


**Figure 12.** Dark matter fraction as a function of radius for different redshifts (coloured lines). The black arrows indicate the half-light radii of the BCGs' most massive progenitors at  $z = 2$  and the red arrows those of the final BCG at  $z = 0$ . *Left:* Dark matter fraction for Ph-C-2. The dark matter fraction increase is substantial: the most massive progenitor at  $z = 2$  had a dark matter fraction of 0.1 (shown where the black arrow intersects the dark blue solid line) within its half-light radius which increased to 0.8 by  $z = 0$  (where the red arrow intersects the orange solid line). *Right:* Dark matter fraction for Ph-E-2. The dark matter fraction within the half-light radius of this galaxy increases mildly from 0.65 at  $z = 0$  to 0.75 by  $z = 0$ . Note that the dark matter fraction decreases substantially in the innermost region of this galaxy (by a factor of 2 within 1 kpc due to a merger with a satellite with much higher central stellar density).

binary: surprisingly this result depended only weakly on the mass ratio  $q = M_1/M_2$  of the black holes or on the inner structure of the stellar density distribution. Assuming that after each of a series of  $N$  mergers with  $M_2 \ll M_\bullet$  the black holes coalesce to a new central object, he estimated the cumulative mass deficit as  $M_{\text{def}} = 0.5NM_\bullet$ , where  $M_\bullet$  is the final mass of the black hole.

We apply this to Ph-E-2 by identifying  $M_\bullet$  as the total mass of all the black holes assigned to the  $z = 2$  progenitor galaxies which merge to the centre of the BCG. We then compare this to the enclosed total mass within 3, 2, 1 kpc. If all black-holes were to merge, this final black-hole mass would be  $M_{BH} = 6.0 \times 10^{10} M_\odot$ . We will assume that after the first merger, a binary black hole is formed with mass  $M_{12} = M_1 + M_2$ . In this case  $M_{12} = 2 \times 10^{10} M_\odot$ . We also note that the black holes involved in subsequent mergers have  $M \ll M_{12}$ . So given that  $N = 4$  further mergers occurred at the centre of the BCG, our estimated deficit mass would be  $M_{\text{def}} \sim 0.5NM_\bullet \sim 12.0 \times 10^{10} M_\odot$ . This could easily account for a core radius of at least 3 kpc, given that the simulated merger remnant has  $M(r < 3 \text{kpc}) = 1.0 \times 10^{11} M_\odot$ . Such large cores are visible in some BCGs (Postman et al. 2012) and, based on this experiment, can be well accounted for in  $\Lambda$ CDM.

Proceeding in a similar way for Ph-C-2, we identify six mergers. Given the  $z = 2$  progenitors in this system, these would lead to a final black hole mass of  $M_\bullet \sim 7.4 \times 10^{10} M_\odot$  and a corresponding mass deficit of  $M_{\text{def}} \sim 0.5NM_\bullet \sim 1.8 \times$

$10^{11} M_\odot$ . Again, this is enough to explain core sizes of 3 kpc or more, given that  $M(r < 4 \text{kpc}) = 2.0 \times 10^{11} M_\odot$  in this BCG. For both clusters we show the radii where mass deficits may affect the distribution of matter in Figures 6 and 7.

We stress however, that these estimates assume that all the black holes coalesce in a series of binary mergers. This may not be the case since triple systems could form and lead to sling-shot ejection of one or all black holes Mikkola & Valtonen (1990). This would result in smaller values of  $M_\bullet$  but larger values of  $M_{\text{def}}$  because multiple black hole systems are more efficient than a binary to move stars around (Merritt et al. 2004; Boylan-Kolchin et al. 2004). Gas may also be expected in some of the progenitor galaxies (given constraints on the fraction of quiescent galaxies at  $z = 2$  (Muzzin et al. 2013)) hastening the coalescence of some binaries, but also promoting the formation of stars and hence smaller mass deficits. Of course, the  $z = 2$  star-forming galaxies may already have lost their gas by the time of the merger, which would eliminate such dissipational effects.

These back-of-the-envelope calculations based on our experiments suggest that black holes may play an important role in the re-distribution of matter within the inner  $\sim 3$  kpc of BCGs, reducing the densities of both stars and dark matter in these regions. This would improve the agreement of the experiments of this paper with the observational data of Newman et al. (2013a) and so would be an interesting topic for further investigation.

## 6 DISCUSSION

Earlier work on this topic has argued that dark matter cusps in the inner regions of clusters will be weakened by energy input from dynamical friction as galaxies merge into the central object, but has failed to be fully convincing through overly idealised treatments and the lack of full gravitational consistency (El-Zant et al. 2004; Nipoti et al. 2004; Laporte et al. 2012). Our current experiments do not suffer from such strong approximations and have been designed to test the importance of dissipationless mixing processes at the centre of galaxy clusters in a realistic cosmological context. Our set-up assumes that at late times the assembly of the inner regions of galaxy clusters is entirely dominated by collisionless merger processes. This is motivated by theoretical work on the formation and evolution of BCGs (De Lucia & Blaizot 2007; Laporte et al. 2013) which appears consistent with observed evolution (Gonzalez et al. 2005; Stott et al. 2011; Lidman et al. 2012). Such an assumption makes the problem well-posed and addressable through N-body simulations: present-day BCGs should be formed from the population of galaxies observed at  $z = 2$  by dynamical processes acting in the concordance  $\Lambda$ CDM cosmology. The consistency of our results with the BCG structure which Newman et al. (2013a) infer for a massive cluster sample including both cool-core and non-cool-core clusters suggests that dissipationless assembly may indeed dominate the late-time growth in all clusters. We note in passing that AGN feedback may also act to produce shallow dark matter cusps (e.g. Martizzi et al. 2012), but current results are not quantitatively convincing because proper hydrodynamical modelling is not possible at full resolution and predictions are highly resolution-dependent (Choi et al. 2014). Feedback effects on the dynamics of stars and dark matter at the centres of galaxies are undoubtedly an interesting area for further investigations.

Our initial conditions were created through impulsively adding stars at the centres of  $z = 2$  dark matter haloes. This causes a transient re-virialisation phase and a compression of the inner regions of the final equilibrium halo. The extent of such compression for realistic galaxy formation models has long been debated (see, for example, the discussion in Tissera et al. 2010). It is clear, however, that the inner total mass profiles of our initial galaxies at  $z = 2$  lie well above the NFW expectations in a dark-matter-only simulation, both because of this compression and because of the added stars. This makes it all the more remarkable that multiple dissipationless mergers can reshape the central mass distribution in the cores of galaxy clusters so that the total mass ends up with an NFW profile and the dark matter distribution has a shallower central cusp.

Below  $r \sim 4\text{kpc}$  our simulations are unable to predict the  $z = 0$  density structure of matter realistically because we do not include the effects of supermassive central black holes. Currently, this problem is difficult to address in cosmological simulations because of the very high spatial and mass resolution which it requires. However, we have estimated how much mass (both dark matter and stars) may be pushed out of the inner regions by black hole mergers, based on the study of Merritt (2006). Such effects are predicted to impose an apparent core with radius  $r \sim 3\text{kpc}$  and to reduce mass densities even at somewhat larger radii.

This has implications for the dark matter annihilation signal predicted from cluster centre Gao et al. (2012). When black hole effects are included, the number of mergers we see in our simulations is sufficient to explain even the largest stellar cores observed in some BCGs Postman et al. (2012).

Our experiments do not fully validate the attractor hypothesis of Loeb & Peebles (2003) because the innermost regions of our final clusters (which are entirely dominated by stars from one or two galaxies) do not follow the profiles found in the dark-matter-only runs. The profiles are, however, similar in the two cases in the regions where there is significant mixing between dark matter and stars. Observed galaxy structure at high redshift ( $z \sim 2$ ) covers a wide range of sizes at given stellar mass (an order of magnitude roughly), but clearly a much broader range (or a very different one) is possible in principle. Thus the near ‘‘universal’’ profile we recover may be related to the particular way in which stellar structure scales with halo mass. It is thus hard to assess whether an attractor exists under more general conditions. An idealised experiment of the sort carried out by Arad & Lynden-Bell (2005), but considering a family of cuspy models, could shed light on this question. Nevertheless, it is interesting to see that the profiles observed by Newman et al. (2013a,b) are very close to those expected in a  $\Lambda$ CDM universe where high-redshift galaxies have the structure observed at  $z = 2$  and the subsequent assembly of BCGs occurs purely through the dissipationless mergers predicted by the  $\Lambda$ CDM model.

## 7 CONCLUSION

We have presented a series of collisionless N-body resimulations of the growth of rich galaxy clusters between  $z = 2$  and  $z = 0$ . We show that dissipationless mergers are expected to produce shallow dark matter cusps consistent with the recent detailed study of Newman et al. (2013b). The profiles in our simulated clusters drop below the NFW expectation at  $r/r_{200} \sim 0.1–0.2$ , as observed. These radii are close to the half-light radii of the BCGs. At smaller radii, the dark matter profiles in our simulations including stars are shallower by  $\Delta\gamma \sim 0.3 – 0.4$  than in their dark-matter-only counterparts, despite the fact that these profiles were actually steeper in the initial  $z = 2$  galaxies. Multiple dissipationless mergers have a strong effect on the dark matter and stellar distributions and lead naturally to the striking result of Newman et al. (2013b) that the *total* mass profile (stars + dark matter) in the cluster core has near-NFW form, and is close to that found in dark-matter-only simulations. Our agreement with observation breaks down in the inner few kpc, but we argue that mergers between the supermassive black holes found in the centres of all massive galaxies are expected to reshape the stellar (and dark matter) distribution of the BCG within 3–4 kpc, giving rise to the observed cores.

An interesting aspect of our simulations is the illustration that the apparent universality of dark matter density profiles may not be set entirely by the physics of early virialisation but may also reflect energy exchange during subhalo mergers. In our case, the increased mass density near the centre of our initial objects is substantially weakened by subsequent mergers so that the total density profile asymptotically

totes back to that found for evolution from unmodified (i.e. dark-matter-only) initial conditions. The challenge in understanding the emergence of this universal solution at a more detailed level is related to analysing the competing effects of dynamical friction, which transfers energy from inspiralling clumps to the diffuse background, and of tidal stripping of the clumps, which adds new material to the diffuse background. In any case, our numerical experiments suggest that the total density profiles measured by Newman et al. (2013a) can be interpreted as validating the galactic cannibalism scenario proposed as the formation channel of BCGs by Ostriker & Tremaine (1975) and White (1976).

## ACKNOWLEDGMENTS

CL was supported in part by the Marie Curie Initial Training Network CosmoComp (PITN-GA-2009-238356). SW was supported in part by ERC Advanced Grant 246797, “Galformod”. CL is supported by a Junior Fellow award from the Simons Foundation. CL would like thank Thorsten Naab, Carlos Frenk, Julio Navarro for useful discussions during the beginning of this project and Scott Tremaine for his comments on an earlier draft.

## REFERENCES

- Arad I., Lynden-Bell D., 2005, MNRAS, 361, 385  
 Barnes J. E., 2012, MNRAS, 425, 1104  
 Bennert V. N., Auger M. W., Treu T., Woo J.-H., Malkan M. A., 2011, ApJ, 742, 107  
 Boylan-Kolchin M., Ma C.-P., Quataert E., 2004, ApJL, 613, L37  
 Choi E., Ostriker J. P., Naab T., Oser L., Moster B. P., 2014, ArXiv e-prints  
 De Lucia G., Blaizot J., 2007, MNRAS, 375, 2  
 Dehnen W., 2005, MNRAS, 360, 892  
 Dubinski J., 1998, ApJ, 502, 141  
 El-Zant A. A., Hoffman Y., Primack J., Combes F., Shlosman I., 2004, ApJL, 607, L75  
 Gao L., Frenk C. S., Jenkins A., Springel V., White S. D. M., 2012, MNRAS, 419, 1721  
 Gao L., Loeb A., Peebles P. J. E., White S. D. M., Jenkins A., 2004, ApJ, 614, 17  
 Gao L., Navarro J. F., Frenk C. S., Jenkins A., Springel V., White S. D. M., 2012, MNRAS, 425, 2169  
 Gonzalez A. H., Zabludoff A. I., Zaritsky D., 2005, ApJ, 618, 195  
 Hernquist L., 1990, ApJ, 356, 359  
 Kazantzidis S., Magorrian J., Moore B., 2004, ApJ, 601, 37  
 Kuijken K., Dubinski J., 1994, MNRAS, 269, 13  
 Laporte C. F. P., White S. D. M., Naab T., Gao L., 2013, ArXiv e-prints  
 Laporte C. F. P., White S. D. M., Naab T., Ruszkowski M., Springel V., 2012, MNRAS, 424, 747  
 Lidman C., Suherli J., Muzzin A., Wilson G., Demarco R., Brough S., Rettura A., Cox J., DeGroot A., Yee H. K. C., Gilbank D., Hoekstra H., Balogh M., Ellingson E., Hicks A., Nantais J., Noble A., Lacy M., Surace J., Webb T., 2012, MNRAS, 427, 550  
 Loeb A., Peebles P. J. E., 2003, ApJ, 589, 29  
 Martizzi D., Teyssier R., Moore B., Wentz T., 2012, MNRAS, 422, 3081  
 Merritt D., 2006, ApJ, 648, 976  
 Merritt D., Milosavljević M., Favata M., Hughes S. A., Holz D. E., 2004, ApJL, 607, L9  
 Mikkola S., Valtonen M. J., 1990, ApJ, 348, 412  
 Moster B. P., Naab T., White S. D. M., 2013, MNRAS, 428, 3121  
 Muzzin A., Marchesini D., Stefanon M., Franx M., McCracken H. J., Milvang-Jensen B., Dunlop J. S., Fynbo J. P. U., Brammer G., Labb   I., van Dokkum P. G., 2013, ApJ, 777, 18  
 Navarro J. F., Eke V. R., Frenk C. S., 1996, MNRAS, 283, L72  
 Navarro J. F., Frenk C. S., White S. D. M., 1997, ApJ, 490, 493  
 Navarro J. F., Ludlow A., Springel V., Wang J., Vogelsberger M., White S. D. M., Jenkins A., Frenk C. S., Helmi A., 2010, MNRAS, 402, 21  
 Newman A. B., Treu T., Ellis R. S., Sand D. J., 2011, ApJL, 728, L39  
 Newman A. B., Treu T., Ellis R. S., Sand D. J., 2013, ApJ, 765, 25  
 Newman A. B., Treu T., Ellis R. S., Sand D. J., Nipoti C., Richard J., Jullo E., 2013, ApJ, 765, 24  
 Newman A. B., Treu T., Ellis R. S., Sand D. J., Richard J., Marshall P. J., Capak P., Miyazaki S., 2009, ApJ, 706, 1078  
 Nipoti C., Treu T., Ciotti L., Stiavelli M., 2004, MNRAS, 355, 1119  
 Ostriker J. P., Tremaine S. D., 1975, ApJL, 202, L113  
 Pontzen A., Governato F., 2013, MNRAS, 430, 121  
 Postman M., Lauer T. R., Donahue M., Graves G., Coe D., Moustakas J., Koekemoer A., Bradley L., Ford H. C., Grillo C., Zitrin A., Lemze D., Broadhurst T., Moustakas L., Ascaso B., Medezinski E., Kelson D., 2012, ApJ, 756, 159  
 Rudick C. S., Mihos J. C., McBride C., 2006, ApJ, 648, 936  
 Ruszkowski M., Springel V., 2009, ApJ, 696, 1094  
 Sand D. J., Treu T., Ellis R. S., 2002, ApJL, 574, L129  
 Sand D. J., Treu T., Ellis R. S., Smith G. P., Kneib J., 2008, ApJ, 674, 711  
 Sand D. J., Treu T., Smith G. P., Ellis R. S., 2004, ApJ, 604, 88  
 Springel V., White S. D. M., Jenkins A., Frenk C. S., Yoshida N., Gao L., Navarro J., Thacker R., Croton D., Helly J., Peacock J. A., Cole S., Thomas P., Couchman H., Evrard A., Colberg J., Pearce F., 2005, Nature, 435, 629  
 Springel V., White S. D. M., Tormen G., Kauffmann G., 2001, MNRAS, 328, 726  
 Stott J. P., Collins C. A., Burke C., Hamilton-Morris V., Smith G. P., 2011, MNRAS, 414, 445  
 Syer D., White S. D. M., 1998, MNRAS, 293, 337  
 Tissera P. B., White S. D. M., Pedrosa S., Scannapieco C., 2010, MNRAS, 406, 922  
 van der Wel A., Franx M., van Dokkum P. G., Skelton R. E., Momcheva I. G., Whitaker K. E., Brammer G. B., Bell E. F., Rix H.-W., Wuyts S., Ferguson H. C., Holden B. P., Barro 2014, ArXiv e-prints  
 White S. D. M., 1976, MNRAS, 174, 19